CHIN. PHYS. LETT. Vol. 38, No. 6 (2021) 068201

$FeSO_4$ as a Novel Li-Ion Battery Cathode

Jiachao Yang(杨家超)[1], Jian Zou(邹剑)[1], Chun Luo(罗春)[1], Qiwen Ran(冉淇文)[1], Xin Wang(王鑫)[1], Pengyu Chen(陈鹏宇)[1], Chuan Hu(胡川)[1], Xiaobin Niu(牛晓滨)[1], Haining Ji(姬海宁)[1*], and Liping Wang(王丽平)[1,2*]

[1]*School of Materials and Energy, University of Electronic Science and Technology of China, Chengdu 610054, China*
[2]*Tianmu Lake Institute of Advanced Energy Storage Technologies, Changzhou 213300, China*

(Received 17 February 2021; accepted 30 March 2021; published online 25 May 2021)

$FeSO_4$ has the characteristics of low cost and theoretical high energy density (799 $W\cdot h\cdot kg^{-1}$ with a two-electron reaction), which can meet the demand for next-generation lithium-ion batteries. Herein, $FeSO_4$ as a novel high-performance conversion-reaction type cathode is investigated. We use dopamine as a carbon coating source to increase its electronic conductivity. $FeSO_4$@C demonstrates a high reversible specific capacity (512 $mA\cdot h\cdot g^{-1}$) and a superior cycling performance (482 $mA\cdot h\cdot g^{-1}$ after 250 cycles). In addition, we further study its reaction mechanism. The $FeSO_4$ is converted to Fe and Li_2SO_4 during lithium ion insertion and the Fe—Li_2SO_4 grain boundaries further store additional lithium ions. Our findings are valuable in exploring other new conversion-type lithium ion battery cathodes.

DOI: 10.1088/0256-307X/38/6/068201

With the increasing concerns about energy and environmental security, renewable and green energies such as lithium-ion batteries (LIBs) are becoming more attractive.[1–3] After decades of development, LIBs have been widely used in portable devices (smartphones, Pads *et al.*) and electric cars. However, higher energy density LIBs, and especially the cathodes, urgently need to meet the demand for a longer endurance time.[4] Meanwhile, the cost is also a key issue for the commercialization of LIBs. Up to now, researchers have explored a series of cathode materials with both high energy density and low cost, such as Li-rich/Ni-rich layered oxides,[5] spinel oxides and conversion-type fluorides.[6–8] Apart from these cathodes, some polyanionic sulfate compounds also meet the requirements of low cost and high energy densities.[9]

Sulfates have the advantages of non-toxicity and high operation potential, which have drawn a lot of concerns.[10–12] A typical sulfate can be expressed as $M_a(SO_4)_b$ (M = Fe, Cu, V, etc.),[13] where the $[MO_6]$ octahedron and $[SO_4]$ tetrahedron are packaged by oxygen atom point sharing. The strong bonding between S^{6+} and O^{2-} leads to a relatively weak interaction between M^{2+} (or M^{3+}) and O^{2-}, resulting in a lower energy of M^{2+} or M^{3+}.[13,14] In other words, the working potential can be very high when compared with other conversion type cathodes (FeS_2, MnO_2, etc.).[10,11,15] A common sulfate, $Fe_2(SO_4)_3$, was firstly studied by Manthiram *et al.* in 1989.[16] It was found that $Fe_2(SO_4)_3$ has two types of crystal structures (rhombohedral structure and orthorhombic framework) with a specific capacity of 100 $mA\cdot h\cdot g^{-1}$, while the work potential is 3.6 V (vs Li/Li^+). Wu *et al.* further studied the lithium ion insertion/extraction mechanism of the mikasaite-type $Fe_2(SO_4)_3$.[17] At initial discharge, two lithium ions were inserted in the $Fe_2(SO_4)_3$ to obtain $Li_2Fe_2(SO_4)_3$. However, only the second lithium ion was reversible in the subsequent cycles. Another sulfate, $CuSO_4$, also attracted attention because of its high operating voltage.[18] Schwieger *et al.* reported that the working potential for $CuSO_4\cdot 5H_2O$ is 3.2 V (vs Li/Li^+),[14] with a specific capacity of 156 $mA\cdot h\cdot g^{-1}$. They believed that the elimination of the crystal water may degrade its electrochemical performance. Apart from these sulfates, fluoridated sulfates were expected to have a much higher operation voltage because of the strong electronegativity of fluorine.[19,20] $LiFeSO_4F$ was demonstrated to have an operation voltage of 3.6 V (vs Li/Li^+), with a specific capacity of 140 $mA\cdot h\cdot g^{-1}$.[21] Similarly, the introduction of the OH^- group showed a comparable effect. $LiFeSO_4OH$ exhibited an average potential of 3.6 V (vs Li/Li^+) with 0.7 mol reversible lithium lions during insertion/extraction processes.[22] Note that many sulphates have a higher working voltage but lower capacity which leads to unsatisfactory energy density.[23] In addition, Nakayama mentioned that polyanionic salts provide high operating voltages,[24] but they simultaneously lead to low electronic conductivities. The theoretical capacity of $FeSO_4$ for a two-electron conver-

Supported by the Fundamental Research Funds for the Central Universities, China (Grant No. ZYGX2019Z008), and the National Natural Science Foundation of China (Grant No. 52072061).
*Corresponding authors. Email: hainingji@uestc.edu.cn; lipingwang@uestc.edu.cn
© 2021 Chinese Physical Society and IOP Publishing Ltd

sion reaction is 352 mA·h·g^{-1}, and the working potential is 2.27 V according to the Nernst equation. Therefore, $FeSO_4$ is expected to provide an energy density of 799 W·h·kg^{-1}, which is higher than the aforementioned sulfates. However, there are lacks of related reports about $FeSO_4$ as a lithium ion battery cathode.

Herein, $FeSO_4$ is explored as a cathode in high energy density lithium metal batteries. With an expanded voltage window (0.01–3.0 V), it delivers an initial discharge specific capacity of 858 mA·h·g^{-1}, much higher than its theoretical value of 352 mA·h·g^{-1}. Meanwhile, $FeSO_4$ has a reversible capacity of 512 mA·h·g^{-1} and maintains a specific capacity of 482 mA·h·g^{-1} after 250 cycles. $FeSO_4$ undergoes a reversible reaction to Fe and Li_2SO_4. Lithium ions are stored in grain boundaries of Fe and Li_2SO_4 below 0.56 V.

Material Synthesis. $FeSO_4{\cdot}xH_2O$ ($x = 6.3$, Aladdin Industrial Corporation) was sintered in a nitrogen atmosphere at 300℃ for 3 h to obtain anhydrous $FeSO_4$. $FeSO_4$@C was prepared by polydopamine (PDA) coating followed by an annealing process. In a typical procedure, 400 mg $FeSO_4$ was added to 30 ml ethanol and stirred at room temperature for 1 h to prepare solution A. Meanwhile, 60 mg 3-hydroxytryptamine hydrochloride (dopamine HCl, Shanghai Titan Scientific Co. Ltd) was dissolved in 5 ml ethanol to prepare solution B. In addition, 102 mg ferric chloride ($FeCl_3$, Shanghai Titan Scientific Co. Ltd) was dissolved in 5 ml ethanol to prepare solution C. Then, solution B was added dropwise to A and stirred for 1 h. Afterward, solution C was added dropwise in the above mixture and stirred for 12 h. The $FeSO_4$@PDA composites were obtained by centrifuging the mixture with ethanol several times and dried in a vacuum oven at 80℃ for 8 h. Then $FeSO_4$@PDA was sintered at 300℃ for 6 h in nitrogen to obtain $FeSO_4$@C composites.

Material Characterizations. The thermogravimetry analysis (TGA) was conducted on a thermal analyzer (Netzsch STA 449C) under a nitrogen atmosphere with a heating rate of 5 ℃/min. The crystal structure was analyzed by x-ray diffraction (XRD, Bruker D8 Advance). Microstructures were examined using the transmission electron microscope (TEM, FEI Talos F200x). Morphologies were carried out by a scanning electron microscope (SEM, Hitachi S-4800).

To value their conductivity, the samples were pressed into a pellet with a diameter of 13 mm under a pressure of 30 kN. The thickness of the $FeSO_4$ and $FeSO_4$@C composites tablets is 1.002 mm and 0.725 mm, respectively. The conductivity was calculated by Ohm's law.

Electrochemical Characterizations. The active material, super P, and polyvinylidene fluoride (PVDF) in N-methyl pyrrolidone (NMP) were mixed in the weight ratio of 6 : 3 : 1 to make a homogenous slurry. The electrodes were prepared by coating the mixture on the copper foil and then vacuum drying (80℃, 12 h). The mass loading is about 2 mg/cm^2. The coin cells were assembled in an argon-filled glovebox. Metallic lithium was used as an anode, celgard 2400 was used as the separator, and 1M $LiPF_6$ dissolved in ethylene carbonate (EC)/dimethyl carbonate (DMC) with a 1 : 1 volume ratio was used as the electrolyte. The specific capacity for $FeSO_4$@C composites is based on a sum weight of $FeSO_4$ and carbon. The *ex situ* XRD patterns were measured with electrodes after cycling. The electrodes were discharged to the corresponding voltage of each state (A–G) at a current density of 0.5 C.

Galvanostatic intermittent titration technique (GITT) was performed on LANHE CT2001A (LAND Electronic Co. Ltd) battery test system. In detail, cells were cycled at a current density of 0.5 C (1 C = 352 mA·g^{-1}) with a voltage window of 0.01–3.0 V, and the cells were charge/discharged for a duration time of 5 min and a relaxation period of 2 h. The cyclic voltammetry (CV) was obtained using the CHI660E (CH Instruments) electrochemical workstation. The scanning rate was 0.1 mV·s^{-1}. The electrochemical impedance spectroscopy (EIS) measurements were carried out with the same instrument. The amplitude was set as 5 mV with frequency range from 1×10^5 to 1×10^{-2} Hz.

Results and Discussion. $FeSO_4{\cdot}xH_2O$ is heated from room temperature to 750℃ in nitrogen at a heating rate of 5℃/min. The TGA curve is shown in Fig. 1(a). With the increase of temperature, the decomposition process of $FeSO_4{\cdot}xH_2O$ as it turns into Fe_2O_3 can be expressed as follows:

$FeSO_4{\cdot}7H_2O$ (room temperature) $\rightarrow FeSO_4{\cdot}xH_2O$ (<77 ℃) $\rightarrow FeSO_4{\cdot}5H_2O$ (86–140 ℃) $\rightarrow FeSO_4{\cdot}H_2O$ (213–260 ℃) $\rightarrow FeSO_4$ (500–650℃) $\rightarrow Fe_2O_3$.

Based on the weight loss, the value of x is determined to be 6.3.

The XRD pattern in Fig. 1(b) confirms that anhydrous $FeSO_4$@C (JCPDS No. 17-0873) can be synthesized by annealing $FeSO_4$@PDA at 300℃ for 6 h. The corresponding crystal structure is also shown in the inset. The basic structural unit of $FeSO_4$ is composed of iron oxide octahedron and sulfur oxygen tetrahedron. The iron element and sulfur element share the oxygen atom. This is a kind of layered structure with 3D lithium-ion channels, which can facilitate the transport of lithium ions. The carbon content in $FeSO_4$@C is calculated to be 8.9 wt% in Fig. S1 in the Supporting Information, and conductivities are calculated by Ohm's law. In Fig. 1(c), the resistances of $FeSO_4$ and $FeSO_4$@C composites are $10^9\ \Omega$ and $1.34 \times 10^5\ \Omega$, respectively. Thus, the $FeSO_4$ exhibits a conductivity of less than 10^{-9} S/m, four orders of magnitude lower

than that of $FeSO_4$@C composites (3.78×10^{-5} S/m). This result shows that carbon coating can improve the conductivity of $FeSO_4$.[25] The morphologies of $FeSO_4$@C are shown in Figs. 1(d)–1(e). Figure 1(d) reveals that $FeSO_4$@C composites are irregular particles with particle sizes less than 100 μm. In Fig. 1(e), many pores are observed, which can be assigned to the crystal water vapor vent during the annealing. In Fig. 1(f), an amorphous surface on $FeSO_4$ can be attributed to the carbon layer. Its thickness is estimated to be 3.1 nm. In addition, the crystallized part can be assigned to $FeSO_4$. The interlayer distance of 0.27 nm corresponds to its (111) plane.

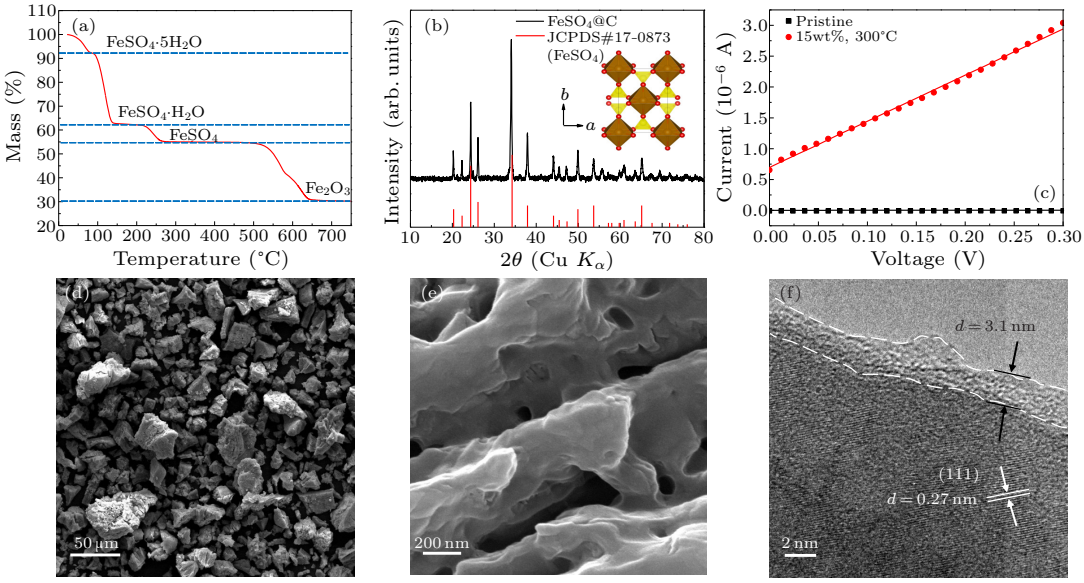

Fig. 1. (a) TGA curve of $FeSO_4 \cdot xH_2O$ ($x = 6.3$) in N_2 at a heating rate of 5 ℃/min. (b) XRD pattern and crystal structure of $FeSO_4$@C composites. (c) The conductivity of $FeSO_4$@C composites and pristine $FeSO_4$. (d) and (e) SEM images of $FeSO_4$@C composites at different magnifications. (f) TEM image of $FeSO_4$@C.

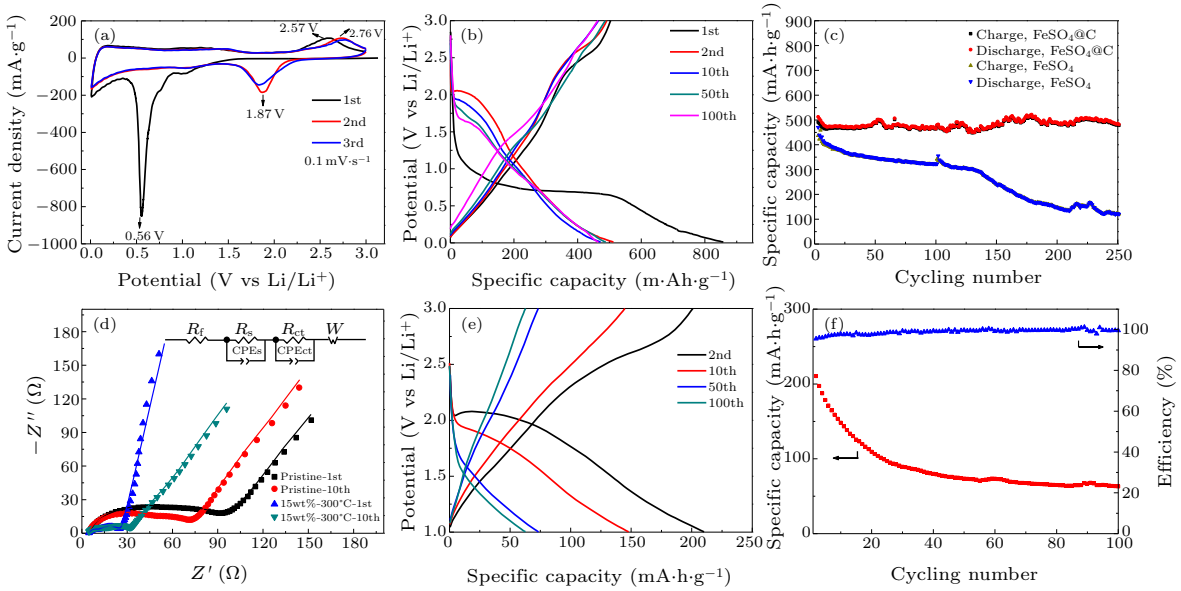

Fig. 2. (a) C–V curves of the $FeSO_4$@C at 0.1 mV/s. (b) Charge/discharge profiles of $FeSO_4$@C (0.01–3.0 V). (c) Cycling performance of the $FeSO_4$@C and pristine $FeSO_4$. (d) EIS of the $FeSO_4$@C and $FeSO_4$. (e) Charge/discharge curves of $FeSO_4$@C (1.0–3.0 V from the 2nd cycle). (f) Cycling performance of $FeSO_4$@C (1.0–3.0 V from the 2nd cycle).

Figure 2(a) shows the C–V curves of $FeSO_4$@C. For the initial scan, the reduction peak around 1.0 V indicates that $FeSO_4$ begins to decompose, and is completely decomposed at the peak of 0.56 V. Meanwhile, it is also accompanied with the formation of solid electrolyte interphase (SEI). The broad oxidation peak is located at 2.57 V. The highly overlapped 2nd and 3rd scans exhibit excellent reversibility. The

oxidation peak and reduction peak are located at 2.76 V and 1.87 V, respectively, indicating that $FeSO_4$ is converted to Fe and Li_2SO_4 during the reduction while $FeSO_4$ is recovered during the oxidation. A detailed discussion will be conducted later. The misalignment between redox peaks indicates a voltage hysteresis, which is related to asymmetrical reaction pathways and sluggish kinetics.[7] Figure 2(b) displays the charge/discharge curves of $FeSO_4$@C at 0.5 C (0.01–3.0 V). The initial discharge capacity is 858 $mA{\cdot}h{\cdot}g^{-1}$. In the subsequent cycles, the lithium ion insertion reaction mechanism is slightly different from the initial cycle. The 2nd discharge capacity is 512 $mA{\cdot}h{\cdot}g^{-1}$, and the efficiency is 91% after 100 cycles (467 $mA{\cdot}h{\cdot}g^{-1}$). The irreversible capacity loss (346 $mA{\cdot}h{\cdot}g^{-1}$) in the initial discharge is attributed to the formation of the SEI layer.[26] Figure 2(c) compares the cycle performance of $FeSO_4$ and $FeSO_4$@C at 0.5 C. After 250 cycles, the capacity of pristine $FeSO_4$ fades (120.7 $mA{\cdot}h{\cdot}g^{-1}$) rapidly while $FeSO_4$@C exhibits excellent stability (482 $mA{\cdot}h{\cdot}g^{-1}$). This is due to the carbon coating, which increases the electronic conductance and suppresses the potential volume change during the conversion reaction of $FeSO_4$. AC impedance is employed to reveal the fading mechanism by analyzing their resistance variations. Figure 2(d) shows the testing and fitting results of EIS. The intercept between the semicircle and the x-axis is the inherent impedance R_f of the battery. In the high-frequency region, the curve is composed of two partially stacked semicircles. The first semicircle is the SEI impedance (R_s//CPE_s), while the second semicircle represents the charge transfer resistance (R_{ct}//CPE_{ct}). In the low-frequency region, the straight line represents Warburg impedance W, which is related to the lithium-ion diffusion. The charge transfer resistance of $FeSO_4$ decreases in the initial 10 cycles. This behavior can be explained by the activation of $FeSO_4$ originating from electrolyte infiltration.[3] Note that $FeSO_4$@C shows smaller resistances in both 1st and 10th cycles. This result demonstrates that the carbon layer can efficiently reduce the charge transfer resistance and leads to better rate performance.

The influence of voltage window between 1.0–3.0 V is also studied. The initial voltage window is 0.01–3.0 V, which is to trigger the decomposition of $FeSO_4$ and the initial capacity is 874 $mA{\cdot}h{\cdot}g^{-1}$. Figure 2(e) is the charge/discharge curves at a current rate of 0.5 C (1.0–3.0 V from 2nd cycle), and the cycle performance is shown in Fig. 2(f). The discharge capacity of $FeSO_4$@C composites is about 210 $mA{\cdot}h{\cdot}g^{-1}$ at the 2nd cycle, while the discharge capacity after 100 cycles is only 63 $mA{\cdot}h{\cdot}g^{-1}$ at 0.5 C. Obviously, the capacity and the cycling stability between 1.0–3.0 V are worse than 0.01–3.0 V. The reason is not yet clear. It seems that grain boundary storage in the low voltage range contributes significantly to the cycle stability. Thus, for a higher capacity and energy density, using 0.01–3.0 V as the voltage range would be more proper.

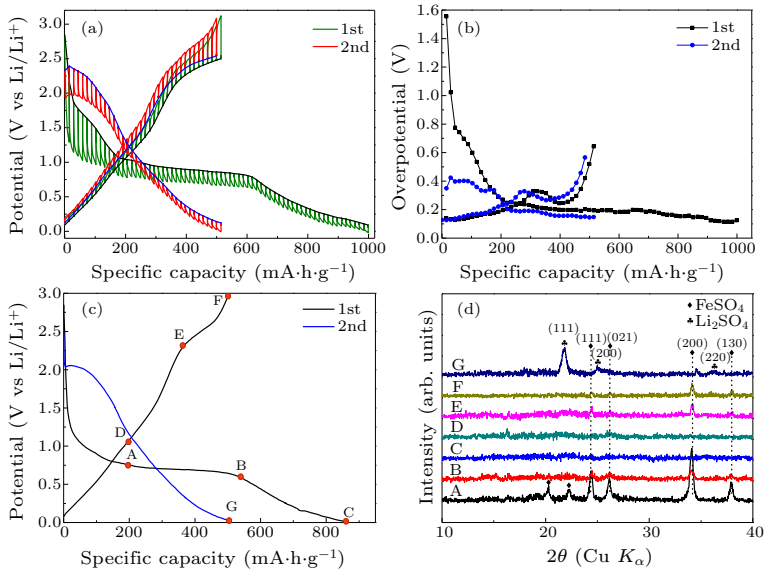

Fig. 3. (a) GITT curves of $FeSO_4$@C at a constant current at 0.5 C for 5 min and a relaxation of 2 h. (b) Polarization voltages as a function of specific capacity. (c) Specific state (A–G) for *ex situ* XRD tests. (d) The *ex situ* XRD patterns at specific states (A–G).

GITT measurements are used to determine the kinetic characteristics of $FeSO_4$@C. The curves of the first 2 cycles are shown in Fig. 3(a). In the GITT model, the discharge capacity increases to 999 $mA{\cdot}h{\cdot}g^{-1}$ at the initial cycle and 514 $mA{\cdot}h{\cdot}g^{-1}$ at the 2nd cycle. Figure 3(b) shows the overpotential variation during the cycling. At the early stage of initial discharge, the overpotential reaches up to

1.6 V. This value gradually decreases with insertion of lithium ions. At the end of the discharge, the overpotential is only 0.2 V. This overpotential drop can be attributed to the generation of Fe during the conversion process that is helpful for improving the conductivity. Thus, with Fe gradually disappearing in the charging process, the overpotential increases. Note that the overpotential of the second discharge is smaller than the initial discharge. This behavior is due to the nanosize effect after the discharge process.[27]

To study the charge/discharge mechanism of $FeSO_4$, *ex situ* XRD patterns are collected at different stages of charge and discharge. Figures 3(c) and 3(d) show the specific states (A–G) and their corresponding XRD patterns, respectively. During the discharge process, the $FeSO_4$ gradually disappears (A $\rightarrow$ B). This process can be simply expressed as follows:

$$FeSO_4 + 2Li \rightarrow Fe + Li_2SO_4. \quad (1)$$

Note that the theoretical capacity of this reaction is only 352 mA·h·g^{-1}, while the experimental value at state B is 530 mA·h·g^{-1}. Considering the SEI layer would generate within the voltage range (<1.0 V), this extra capacity can be attributed to the formation of SEI.[28] Moreover, the theoretical potential of reaction (1) calculated by the Nernst equation is 2.27 V,[18] corresponding to the theoretical energy density of 799 W·h·kg^{-1}. However, it is observed that the initial discharge plateau is below 2.0 V in Fig. 3(a), much lower than the theoretical value. Such a deviation shows that the overpotential is needed to initiate and to pursue the decomposition reaction.[29] This phenomenon is quite common in conversion type materials.[29,30] Indeed, there is no obvious Fe and Li_2SO_4 reflections at state B, which confirms that these two products are amorphous. With a further lithium-ion insertion (B $\rightarrow$ C), there would be a long voltage slope. This slope has been widely observed in other conversion type materials. The different fermi levels of Fe and Li_2SO_4 particles make their grain boundaries highly reactive and thus enable extra lithium ion insertions.[31] The storage mechanism is known as the "job-sharing",[32] where the electrons are accommodated by Fe and the lithium ions are stored in Li_2SO_4. Thus, the reaction between 0.01 V and 0.56 V can be expressed as

$$Fe + Li_2SO_4 + xLi \rightarrow Fe|xLi|Li_2SO_4. \quad (2)$$

During the charging process, there is no obvious changes in the XRD patterns for C $\rightarrow$ D, corresponding to the lithium ion extraction from the Fe—Li_2SO_4 grain boundaries. The gradual strength of $FeSO_4$ reflections from D $\rightarrow$ E $\rightarrow$ F indicates that reaction (1) is reversible. Thus, the overall reversible capacity is contributed by the conversion reaction between $FeSO_4$ and Fe+Li_2SO_4, and the Fe—Li_2SO_4 grain boundaries storage.

In summary, the electrochemical properties of $FeSO_4$ as a Li-ion battery cathode and its reaction mechanisms have been revealed. We use a simple carbon coating method to obtain $FeSO_4$@C for improving its conductivity. The $FeSO_4$@C exhibits a high initial discharge specific capacity of 858 mA·h·g^{-1}, with a reversible specific capacity of 512 mA·h·g^{-1} and delivers a specific capacity of 482 mA·h·g^{-1} after 250 cycles (0.01–3.0 V). With *ex situ* XRD tests, it can be concluded that the reversible capacity is contributed by the conversion reaction between $FeSO_4$ and Fe+Li_2SO_4, and due to lithium ion storage between Fe and Li_2SO_4 grain boundaries at low voltage. The research provides a comprehensive understanding of $FeSO_4$ and mechanism studying for other conversion type materials.

References

[1] Harper G, Sommerville R, Kendrick E, Driscoll L, Slater P, Stolkin R, Walton A, Christensen P, Heidrich O, Lambert S, Abbott A, Ryder K S, Gaines L and Anderson P 2019 *Nature* **575** 75

[2] Kim T, Song W, Son D Y, Ono L K and Qi Y 2019 *J. Mater. Chem. A* **7** 2942

[3] Wang H, Lan X, Huang Y and Jiang X 2019 *Chin. Phys. Lett.* **36** 098201

[4] Wu M S, Xu B and Ouyang C Y 2016 *Chin. Phys. B* **25** 018206

[5] Pieczonka N P W, Liu Z, Lu P, Olson K L, Moote J, Powell B R and Kim J H 2013 *J. Phys. Chem. C* **117** 15947

[6] Lee S, Jeong M and Cho J 2013 *Adv. Energy Mater.* **3** 1623

[7] Wang L P, Wu Z R, Zou J, Gao P, Niu X B, Li H and Chen L Q 2019 *Joule* **3** 2086

[8] Chen Y C, Huo M, Liu Y, Chen T, Leng C C, Li Q, Sun Z L and Song L J 2015 *Chin. Phys. Lett.* **32** 017102

[9] Li W, Dolocan A, Oh P, Celio H, Park S, Cho J and Manthiram A 2017 *Nat. Commun.* **8** 14589

[10] Nanjundaswamy K S, Padhi A K, Goodenough J B, Okada S, Ohtsuka H, Arai H and Yamaki J 1996 *Solid State Ionics* **92** 1

[11] Kitajou A, Ishado Y, Inoishi A and Okada S 2018 *Solid State Ionics* **326** 48

[12] Radha A V, Lander L, Rousse G, Tarascon J M and Navrotsky A 2015 *J. Mater. Chem. A* **3** 2601

[13] Shirakawa J, Nakayama M, Wakihara M and Uchimoto Y 2007 *J. Phys. Chem. B* **111** 1424

[14] Schwieger J N, Kraytsberg A and Ein-Eli Y 2011 *J. Power Sources* **196** 1461

[15] Lu J C, Nishimura S and Yamada A 2017 *Chem. Mater.* **29** 3597

[16] Manthiram A and Goodenough J B 1989 *J. Power Sources* **26** 403

[17] Wu Q, Xu Y H and Ju H 2013 *Ionics* **19** 471

[18] Lee Y, Jo C H, Yoo J K, Choi J U, Ko W, Park H, Jo J H, Shin D O, Myung S T and Kim J 2020 *Energy Storage Mater.* **24** 458

[19] Recham N, Rousse G, Sougrati M T, Chotard J N, Frayret C, Mariyappan S, Melot B C, Jumas J C and Tarascon J M 2012 *Chem. Mater.* **24** 4363

[20] Sun Y, Liu L, Dong J P, Zhang B and Huang X J 2011 *Chin. Phys. B* **20** 126101

[21] Recham N, Chotard J N, Dupont L, Delacourt C, Walker

W, Armand M and Tarascon J M 2010 *Nat. Mater.* **9** 68
[22] Subban C V, Ati M, Rousse G, Abakumov A M, Van Tendeloo G, Janot R and Tarascon J M 2013 *J. Am. Chem. Soc.* **135** 3653
[23] Lander L, Tarascon J M and Yamada A 2018 *Chem. Rec.* **18** 1394
[24] Nakayama M, Goto S, Uchimoto Y, Wakihara M, Kitajima Y, Miyanaga T and Watanabe I 2005 *J. Phys. Chem. B* **109** 11197
[25] Chen M, Chen L, Hu Z, Liu Q, Zhang B, Hu Y, Gu Q, Wang J L, Wang L Z, Guo X, Chou S L and Dou S X 2017 *Adv. Mater.* **29** 1605535
[26] Zhong K F, Xia X, Zhang B, Li H, Wang Z X and Chen L Q 2010 *J. Power Sources* **195** 3300
[27] Zou J, Zhao J, Wang B, Chen S, Chen P, Ran Q, Li L, Wang X, Yao J, Li H, Huang J, Niu X and Wang L 2020 *ACS Appl. Mater. Interfaces* **12** 44850
[28] Kim S, Choi J, Bak S M, Sang L, Li Q, Patra A and Braun P V 2019 *Adv. Funct. Mater.* **29** 1901719
[29] Poizot P, Laruelle S, Grugeon S and Tarascon J M 2002 *Electrochem. Soc.* **149** A1212
[30] Reddy M V, Yu T, Sow C H, Shen Z X, Lim C T, Rao G V S and Chowdari B V R 2007 *Adv. Funct. Mater.* **17** 2792
[31] Guo X, Fang X, Mao Y, Wang Z, Wu F and Chen L 2011 *Phys. Chem. C* **115** 3803
[32] Chen C C and Maier J 2018 *Nat. Energy* **3** 102

Supporting Information for "$FeSO_4$ as a Novel Li-Ion Battery Cathode"

Jiachao Yang(杨家超)[1], Jian Zou(邹剑)[1], Chun Luo(罗春)[1], Qiwen Ran(冉淇文)[1], Xin Wang(王鑫)[1], Pengyu Chen(陈鹏宇)[1], Chuan Hu(胡川)[1], Xiaobin Niu(牛晓滨)[1], Haining Ji(姬海宁)[1**], and Liping Wang(王丽平)[1,2**]

[1]School of Materials and Energy, University of Electronic Science and Technology of China, Chengdu 610054, China

[2]Tianmu Lake Institute of Advanced Energy Storage Technologies, Changzhou 213300, China

[*]This work is supported by the Fundamental Research Funds for the Central Universities, China (ZYGX2019Z008) and the National Natural Science Foundation of China (52072061).

[**]Corresponding authors. Email: hainingji@uestc.edu.cn; lipingwang@uestc.edu.cn

The TGA curve of $FeSO_4$@C is shown in Fig. S1. We use TGA measurement to determine the content of C. The decomposition process of $FeSO_4$ in the air can be summarized as follows [1]:

$$2FeSO_4+1/2O_2 \rightarrow Fe_2O_3+2SO_3\uparrow \quad (1)$$

According to Eq. (1), the theoretical weight loss is 47.3 wt.% from $FeSO_4$ to Fe_2O_3. Here, the weight loss is 52.3 wt.% in $FeSO_4$@C (Fig. R1). Thus, the content of C is calculated to be 8.9 wt.%.

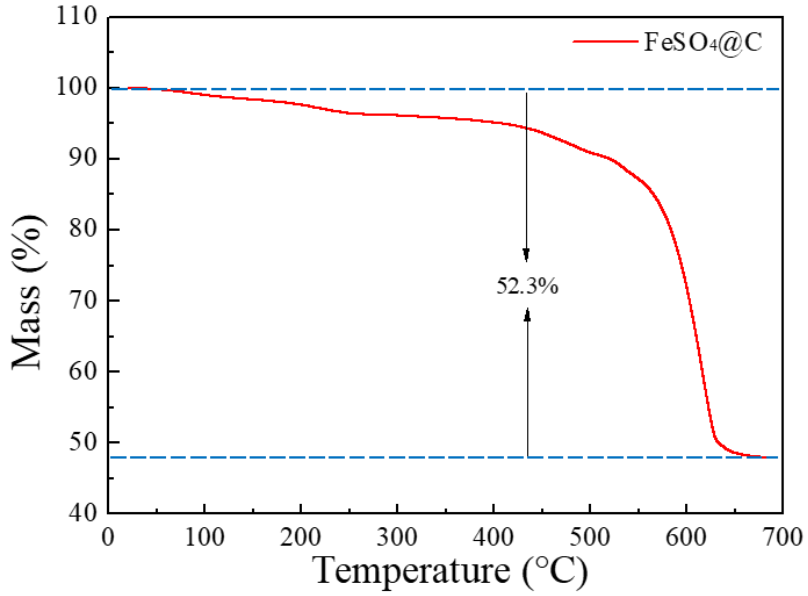

Fig. S1 TGA curve of $FeSO_4$@C in the air at a heating rate of 5°C/min

[1] Gallagher P K, Johnson D W, Schrey F 1970 *J. Am. Ceram. Soc.*53 666